ACS APPLIED MATERIALS & INTERFACES

Research Article

www.acsami.org

Fractal Patterning of Nanoparticles on Polymer Films and Their SERS Capabilities

George Amarandei,*[,†] Colm O'Dwyer,[‡,§,⊥] Arousian Arshak,[†,⊥] and David Corcoran[†]

[†]Department of Physics and Energy and [⊥]Materials and Surface Science Institute, University of Limerick, Ireland

[‡]Department of Chemistry, University College Cork, Ireland

[§]Tyndall National Institute, Lee Maltings, Cork, Ireland

Supporting Information

ABSTRACT: We demonstrate control, via electro-hydrodynamic (EHD) induced polymer instabilities and nanoparticle mobility, of hierarchical fractal arrangements of gold nanoparticles on patterned thin polymer films. The induced changes in the film curvature enhance fractal formation for high and not for low mobility nanoparticles. The high mobility nanoparticles cluster in circular fractal networks on the rims of a hexagonally ordered array of EHD-induced polymer peaks. These arrangements exhibit plasmonic properties for surface-enhanced Raman scattering (SERS) spectroscopy.

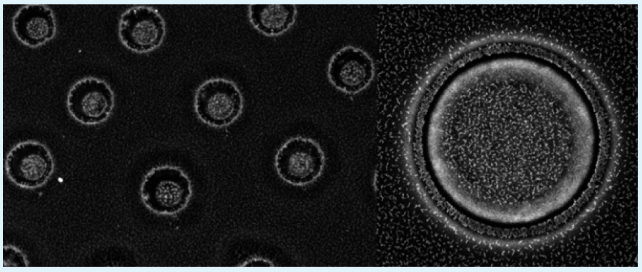

KEYWORDS: *nanoparticles, thin polymer films, electro-hydrodynamic instabilities, patterning, SERS*

INTRODUCTION

The patterning of nanoparticles (NPs) on surfaces is a prerequisite for nanotechnological applications in photonics, sensing and biomedical science.[1−4] Patterned polymer films containing dielectric NPs have been proven to be viable candidates for a new class of solar cell.[1] Pioneering expertise has been developed in the functional application of nanoparticle polymer film composites[5−9] with potential applications ranging from novel optical and magnetic materials to sensors and even antibacterial coatings.[8] A large variety of reproducible fabrication methods are available for adding nanoparticles to thin-polymer film surfaces, e.g., drop casting from solutions,[6] spray coating,[7] vapor,[8] thermal or sputter deposition.[5] In particular, solvent evaporation arising from drop casting or spray coating can be used to pattern in a controllable manner the nanoparticles on a polymer film.[6,7] These low-cost fabrication methods use evaporation induced self-assembly for achieving gold nanoparticle ensembles and patterning of the thin film simultaneously.

When arranged periodically and/or regularly, metallic NPs are useful for surface enhanced Raman scattering (SERS) that combines noninvasive and nondestructive molecular fingerprint specificity[10] and single-molecule sensitivity.[11] The coupling of surface plasmon polaritons on proximal Au NP surfaces enhances the electromagnetic (EM) field[12] and creates "hot spots" that allow significantly enhanced scattering cross sections and very sensitive detection limits.[13−16]

The ultrasensitivity and potential label-free analysis associated with SERS has made it an attractive and powerful analytical technique to identify and quantify analytes in applications ranging from biosensing and explosive detection to art conservation.[15,16] The main problem in creating "nanoplasmonic devices" is to impregnate/pattern rigid or flexible substrates over large areas with regular arrays of nanoparticles that can exhibit SERS effects.[4,15,17] The patterning has to be done in a simple and repeatable fashion to ensure low manufacturing costs for the development of low-cost plasmonic sensors for daily life applications. In the current state-of-the-art methods, patterning is obtained by means of expensive lithographic techniques (nanotransfer printing, shadow overlap of ion-beam lithography, etc.) or by the development of sophisticated synthesis colloidal techniques.[14−20] Both classes of methods can lead to the desired regular patterns but they are expensive and have low-throughput. A possible alternative is the use of soft-lithographic methods that employ thin polymer nanocomposite films to produce hierarchical patterns.[2−4] By controlling the self-assembly and self-organization properties of matter, regular patterns can be created with limited input from the outside.

At temperatures larger than the glass transition temperature T_g and in the absence of additional external fields, the stability of the films is controlled by the van der Waals forces between the air−polymer and polymer−substrate interfaces.[21−24] For pristine films in a capacitor configuration (with applied electric fields of ∼10−50 V/μm), at $T > T_g$, the electric pressure exerted on the dielectric liquid usually dominates and destabilizes the initially flat air−polymer interface. A process

Received: June 12, 2013
Accepted: August 15, 2013
Published: August 27, 2013

   dx.doi.org/10.1021/am402285e | ACS Appl. Mater. Interfaces 2013, 5, 8655−8662

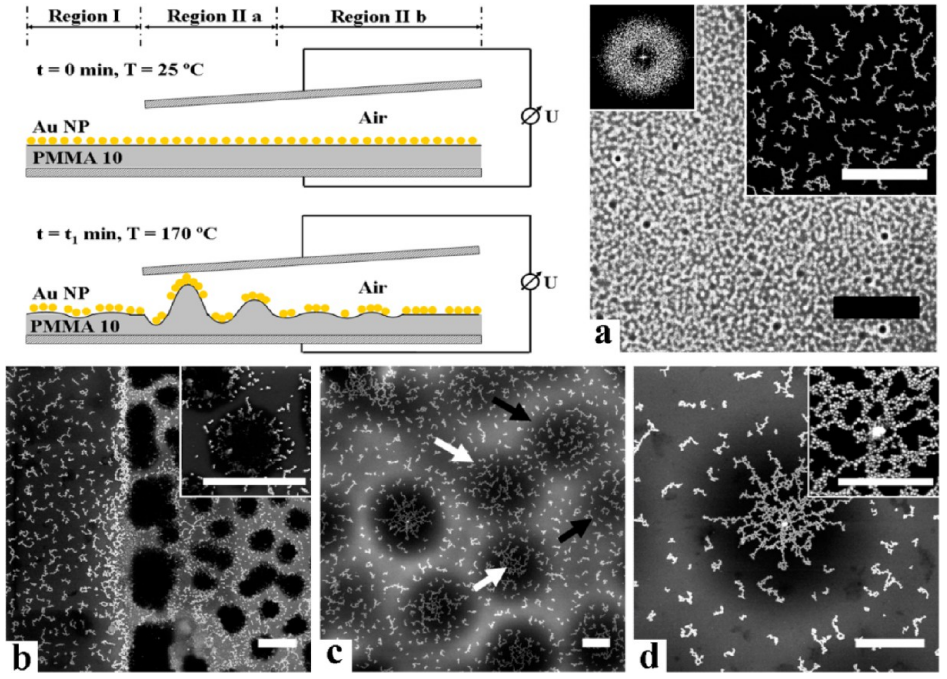

Figure 1. Schematic diagram showing the development of instabilities in a region without and with the electric field. (a) Optical micrograph (scale bar (SB) = 50 μm) of the spinodal instability (as shown by the FFT) developed due to Au coverage in the region without electric field on a film of h_{PMMA10} = 29 nm, h_{Au} = 1 nm after t_1 = 21 min. The SEM inset (SB = 1 μm) shows the Au distribution. (b) SEM image showing the transition from region I to region IIa (SB = 1 μm). The SEM inset (SB = 1 μm) describes the Au distribution in and around a peak of the EHD instability that was already in contact with the top electrode. (c) SEM image (SB = 1 μm) showing the different stages in EHD development at the transition between region IIa and region IIb. The black arrows indicate EHD peaks in the early stages (small amplitude) where the Au particles distribution is closed to that for the flat film. The white arrows indicate the beginning of the fractal cluster formation. (d) SEM image (SB = 1 μm) of a fully formed EHD instability peak in region II showing the changes in particle density. The inset (SB = 500 nm) shows that as the density become larger on the peak and the particles already form a fractal cluster.

of self-organization that leads to pattern formation is triggered.[25−28]

The high electric fields in a capacitor configuration generate interfacial pressures that are strong enough to destabilize the film by overcoming the stabilizing action of the surface tension.[25,28,29] The amplitude of the selected linear mode grows first exponentially, then nonlinear effects set in and the growth continues until the film maxima touch the other substrate of the capacitor. In this way an array of liquid columns that connect the two substrates is formed.[25] The nonlinear growth process and potentially also the electrostatic repulsion between the columns may lead to their arrangement in lattices with different symmetries (e.g., square, hexagonal). Their geometry, however, does not always remain the same over the entire area, and a coexistence of different patterns is sometimes observed.[25,29−31] The packing order of the columns is controlled by the film thickness, and an almost perfect hexagonal distribution is observed for a specific ratio of the film thickness with respect to the air gap in the capacitor.[25,29−31] The use of electric fields can create hierarchical 3D structures in a single step if multilayers of thin polymer films are employed.[4,29,32−36]

The incorporation of nanoparticles with high dielectric constants as fillers in a thin polymer film leads to a systematic reduction in length scales of the induced pattern.[3] Independently of the type of filler, no migration or altering of the structure generated by the electric field is observed.[2,3]

Here, we show that electro-hydrodynamic (EHD) induced instabilities form an array of polymer patterns with unique Au NP fractal distributions. The polymer structures decorated by NP fractal networks exhibit significant SERS for probe organic molecules. The method has the advantage of patterning the polymer and Au NPs simultaneously. This establishes the possibility of creating and controlling Au NP polymer hierarchical structures for use in nanotechnological applications.

EXPERIMENTAL SECTION

Sample Preparation. Si wafers (native oxide, $h_{SiOx} \simeq 2.0$ nm) with a resistivity of 2−3 Ω cm were cleaned in a jet of CO_2 ice crystals, and were used as substrates. For good electrical contact, 5 nm Cr and 40 nm Au films were deposited on the backside of the wafers. Thin poly (methyl-methacrylate) [PMMA10, M_w = 10 kg/mol, R_g = 2.76 nm, M_w/M_n = 1.05, Sigma-Aldrich, UK] and polystyrene [PS10, M_w = 10 kg/mol, R_g = 2.59 nm, M_w/M_n = 1.05, Sigma-Aldrich, UK] films were obtained by spin coating onto the substrates using 2−3% (w/w) polymer solution in toluene.[29]

Gold layers with different nominal thicknesses (as specified for each experiment in the figure captions) were sputtered at a low rate (0.09 nm s^{-1}) onto the polymer thin films creating a Si/SiO_x/polymer/AuNP/air configuration.[5,14,23] The deposition led to initial uniformly random distributed NPs on the polymer surface in the central region of the samples allowing a direct comparison between Si/SiO_x/polymer/air and Si/SiO_x/polymer/AuNP/air regions (see refs 23 and 24 and schematics drawn in the figures). The films were used as cast and deposited, and no annealing procedure was performed prior to heating. All experiments were made in a convection oven at 170 °C. The polymer−air and polymer−air−polymer capacitor configurations (as shown in the different schematic diagrams) were obtained using SiO_2 microspheres of 1 μm diameter that act as spacers.[29] A voltage U = 50 V was applied to perturb the air−polymer interfaces. During the experiments the current through the capacitor was monitored. After an initial transient period during heating, a small constant current was

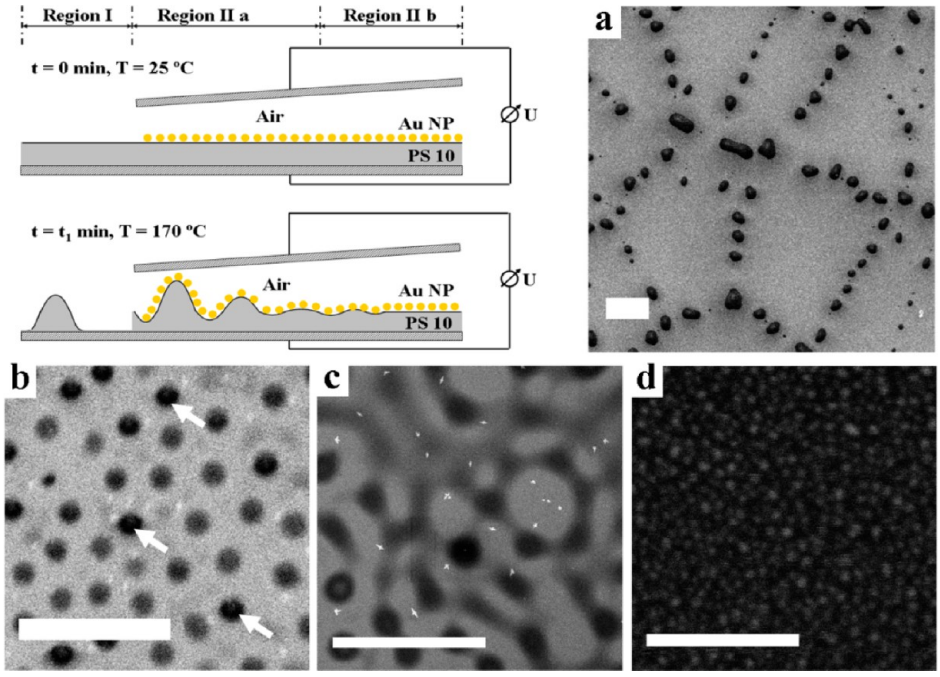

Figure 2. Schematic diagram showing the development of the instability in a region without and with the electric field applied. SEM images describing (a) the nucleation dewetting in the region without Au and electric field (SB = 50 μm); (b) the EHD instability in region IIa (SB = 50 μm). The white arrows indicate some of the contact points with the upper electrode; (c) the early stages of the EHD instability as seen in region IIb (SB = 50 μm) and (d) the uniform distribution that is maintained as deposited in region II (SB = 50 nm). The polymer film thickness h_{PS10} = 25 nm and the nominal thickness of the Au layer h_{Au} = 1 nm. The experimental time is t_1 = 90 min.

observed (1−60 mA). If significant large changes in the current or short-circuits occurred, the sample was disregarded.[29] The samples were removed from the oven and quenched at different time intervals in the presence of the electric field. At the end of the experiment the samples were mechanically separated. For the polymer−air−polymer configuration, the PS was washed from the PMMA substrate using cyclohexane. The SiO_2 spheres were removed by using PDMS stamps.

Electron Microscopy. The polymer films and the Au NP distributions were imaged by electron microscopy using a Hitachi S4800 FESEM operating at 4 kV and a FEI Orion Focused Ion Beam at 5 kV. The mean radius of the particles R_p and the edge-to-edge distance d_{ee} between the nearest neighbors were measured using SPIP and calculated as described in detail elsewhere.[23,24] The initial deposition of a nominal 1 nm thickness of Au led to NPs with $R_p \approx$ 1.74 nm and $d_{ee} \approx$ 1.76 nm respectively (see also refs 23, 24). For a nominal 2 nm Au deposition, presented in Figure 5, the particles were characterized by R_p = 3.48 nm and d_{ee} = 1.79 nm. The fractal dimension D was calculated using the box counting method available in FIJI (see ref 24 for details).

Surface-Enhanced Raman Specroscopy. SERS measurements were carried out using a Horiba Jobin-Yvon T64000 Triple Raman spectrometer attached to an Olympus confocal optical microscope. Excitation was provided by a He−Ne laser with a wavelength λ = 633 nm. The spectra were typically acquired with a 5 s exposure time and a laser power of 5 mW (at 633 nm) to avoid organic dye burning. A 50× objective with a numerical aperture N.A. of 0.75 was used for all Raman scattering measurements. This led to a laser spot size A_{spot} = 1.22 λ/N.A. $\approx$ 1.1 μm^2. Methyl Violet (MV) 10B was used as the probe molecule. The Methyl Violet 10B reagents were dissolved into pure deionized water (18.3 MΩ cm) and ethanol. The patterned sample was immersed for 1 h in the dye solution at a concentration of 1.0×10^{-6} mol dm^{-3} for sufficient molecule adsorption before SERS measurements, and subsequently rinsed with deionized water.

RESULTS

Thin polymer films at temperatures larger than their glass transition temperature become liquid and the Au NPs present at the polymer−air interface become free to diffuse and aggregate.[23,24] To distinguish between the effect of heating with and without the electric field, only a part of the thin PMMA-NP covered system is placed in the capacitor configuration as indicated in the schematic diagram in Figure 1. This allows a direct comparison of the instabilities developed by the NP coverage in region I (Figure 1a) and by the electric field in region II (Figure 1b−d) and the influence these instabilities have on the Au NP distribution.

In region I, the initial stages of the spinodal instability (Figure 1a) are seen. A previously reported fractal network (D = 1.68 ± 0.09) of Au NPs (seen at t > 45 min) that forms as a result of a cluster−cluster limited aggregation process[24] is not observed here. Only its incipient stages, i.e., the formation of quasi-linear NP clusters, which are the main constituents of the eventual NP fractal network, are observed as the experimental time is short ($t_1 \approx$ 21 min). The Au clusters formed during aggregation are uniformly distributed on the peaks and within the troughs of the polymer instability, showing that the development of the spinodal instability does not influence NP movement.

The transition between region I and region II is seen in Figure 1b. In region II, the typical EHD pattern develops by the end of the experiment as observed by the shadow features in the SEM observations (Figure 1b−d). The top electrode of the capacitor is placed at a small angle (exaggerated in the schematic diagram for illustration purposes) and this allows the observation of the EHD instability development at different times without measurable change to the instability wavelength.[4,29] In region IIa where the electric field is larger, the instability develops faster and it is observed in its final development stages after touching the upper electrode (Figure 1b, right), at an intermediate developed stage but not touching the electrode (Figure 1c, left), and in its initial stages in region

dx.doi.org/10.1021/am402285e | ACS Appl. Mater. Interfaces 2013, 5, 8655−8662

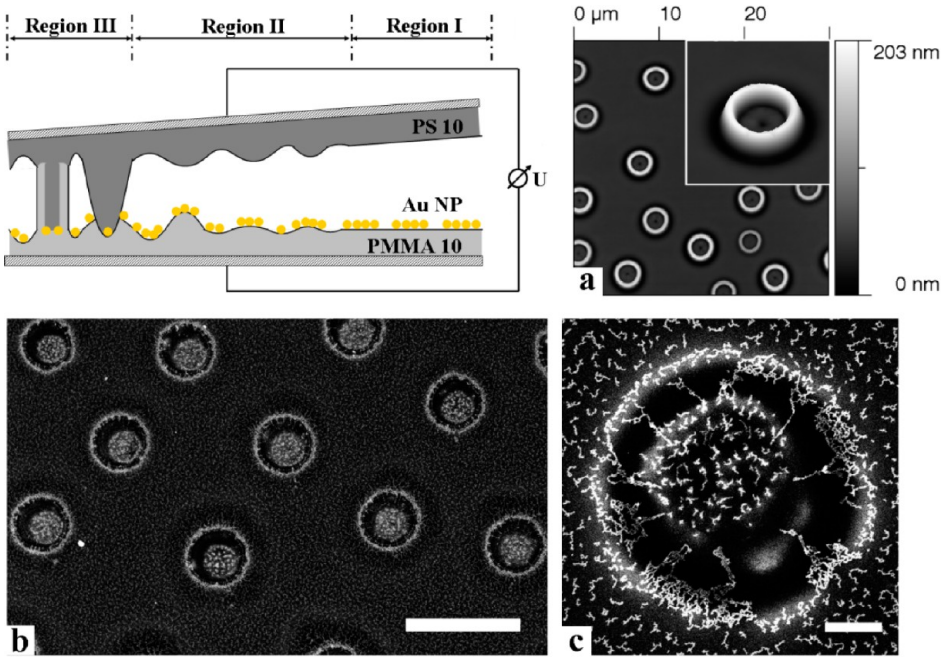

Figure 3. Schematic diagram showing the polymer surface and NP distribution in a polymer/AuNP−air−polymer system. (a) The PMMA surface after PS washing from a PS100-air-PMMA100 as described in ref 16. (b) SEM image (SB = 10 μm) showing the PMMA10 surface and the Au distribution from a PMMA10/AuNP−air−PS10 system. The flat film between the rings indicates the presence of type II behavior.[16] (c) SEM image (SB = 1 μm) showing a magnified view of the rings and emphasizing the presence of the fractal cluster on the rim. The linear clusters have the same distribution inside and outside of the rims. The experimental heating time is t_1 = 28 min.

IIb (Figure 1c, right). The black arrows in Figure 1c reveal the initial stages of the EHD development and associated Au NP distribution. When the amplitude of the instability is small, the particle distribution on the peaks is almost the same as in the instability troughs. However, once the instability grows in amplitude, the particle density on the peaks starts to increase and the quasi-linear clusters begin forming fractal networks (white arrows in Figure 1c). Finally, prior to contact, the fractal network is fully formed and covers the entire peak of the EHD instability as seen to the left of Figure 1c and magnified in Figure 1d and its inset. The network is formed by Au NPs with a mean radius $R_p \approx 5.91$ nm and a mean edge-to-edge distance $d_{ee} \approx 4.51$ nm and it has a fractal dimension of $D = 1.69 \pm 0.11$. Fractal networks of Au NPs are known to arise when the deposited films are near the percolation threshold.[9] The values of fractal dimension compare well with those seen after 135 min of heating in a sample where no electric field was present (see ref 24). Here, however, these values are obtained after shorter time ($t_1 \approx 21$ min).

Thus the EHD induced polymer instability with a characteristic wavelength can be patterned with high and low density distributions of Au NPs and it seems to enhance the cluster−cluster aggregation process that leads to fractal formation.

The experiment is repeated using thin polystyrene films covered by Au NPs where the NP mobility is smaller.[23,24,37,38] In the absence of any other external fields, such films also develop a spinodal instability,[23] but the time to reach full development is much longer than for PMMA. In PMMA films, a spinodal instability can develop in the first ~45 min, reaching its maximum amplitude by ~315 min;[24] in PS films, a spinodal instability requires over 24 h to reach its maximum amplitude.[23] Therefore, the electric field is applied over the entire surface area covered by Au NPs, as schematically described in Figure 2. As in the PMMA study (Figure 1), a small angle (exaggerated in the schematics) exists between the capacitor plates allowing observation of different evolution stages of the EHD instability.

In region I, where no Au NPs or electric field are present (Figure 2a), the thin polymer film exhibits nucleation dewetting and beads up in a Voronoi pattern as expected.[23] In region IIa, the instability is fully formed and its peaks already contact the upper electrode at a few locations (the black points indicated by white arrows in Figure 2b). In region IIb, the early stage of the instability is seen (Figure 2c). Independently of the development stage of the EHD instability or their position (i.e., on the peaks or within the troughs), the Au NPs maintain their initial uniform distribution as seen in Figure 2d. In this regard, as noted earlier, Au NP aggregation occurs at a slower rate on PS than on PMMA, taking place either through Ostwald ripening or a slow coalescence process.[23,39]

In a double-layer PS/air/AuNP/PMMA configuration (Figure 3), a single mode instability is predicted[29] and indeed is experimentally seen to develop in both layers. Because of the higher bulk viscosity of the PMMA film combined with the presence of Au NPs on its surface, its mobility is significantly lower than the mobility of the PS film, and consequently the instability grows faster in the more mobile PS film.[29] Indeed, the topography of the PS-PMMA double layer is consistent with the type II topography previously seen for double-layer systems where the mobility of one film far exceeds that of the other. The more mobile film exhibits a labyrinthine pattern, whereas the less mobile film exhibits features that appear to be extruded from a flat background.[29]

As PS and PMMA are used, columns with a PS core and PMMA shell are formed[29,32,33] when the corrugated peaks of the two polymer films meet (Figure 3a.). In this case, the densification of the Au NPs occurs on and/or around the rims created by the PMMA shells (Figure 3b,c). Where PS peaks contact the AuNP/PMMA layer, the Au NP aggregation

appears to freeze-in (Figure 3b,c) as the Au NPs adsorb to PS.[23,40] As has been shown above, the NP distribution on PS is effectively retarded from significant changes. The result is the generation of a rich hierarchical Au NP−polymer structure (Figure 3.b) consisting of a polymer film plane of uniform Au NP cluster distribution, on which are superimposed polymer rims with high-density Au NPs and inner troughs of Au NP clusters (Figure 3.a).

Different stages of evolution of the Au NPs on polymer patterns are observed due to the slight tilt in the electrode spacing mentioned earlier (see also ref 29). In the more developed situation presented in Figure 3, the fractal network is located on the outside base of the rim. At an earlier stage of development (Figure 4a), the Au NP fractal network (D = 1.73 ± 0.09) is distributed along the entire contour and on the top of the rim (Figure 4b). The particles have a mean $R_p \approx 6.86$ nm and $d_{ee} \approx 4.8$ nm. The particles outside of the rim (see also Figure S1 in the Supporting Information.) form clusters that are not connected to the NP network. The particles within such clusters are characterized by an $R_p \approx 7.26$ nm and $d_{ee} \approx 5.2$ nm. As seen in Figure 1, the cluster−cluster aggregation process is enhanced by the presence of a larger curvature (in this case on the rim).

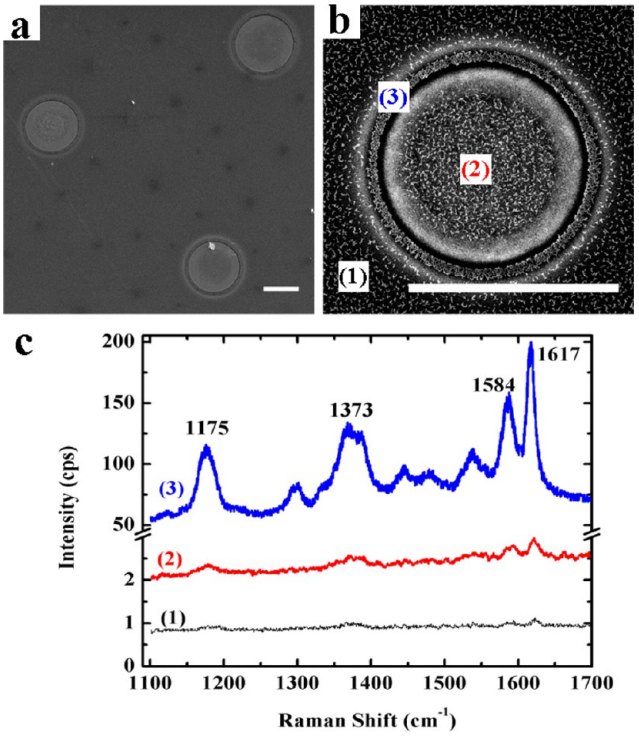

Figure 4. (a) Secondary electron FIB images showing early contact structures in PMMA (SB = 10 μm) after the MV solution is applied; (b) SEM magnification of a PMMA feature (SB = 10 μm) prior to MV adsorption; (c) SERS spectra obtained at the positions identified in (b).

A similar ridge with Au NP densification and an inner trough with uniformly distributed NPs can also be produced by placing a SiO_2 sphere on a heated AuNP/PMMA configuration, as depicted in Figure 5. In this instance, the Au NPs outside the rim form the typical fractal network of Au NP clusters previously observed.[24] The fractal is also present on the rim, but underneath the spheres, *i.e.* where the mobility of the NPs is severely impaired, the distribution remains uniformly random. These results together with the observations from polymer−air and the polymer−air−polymer configurations above suggest that the local increase in the curvature of the polymer extrusions enhances the Au NP organization process to form fractal NP arrangements, while the factors that reduce Au NP mobility act to retard this process.

Site specific SERS measurements are carried out on the early stage PMMA structures from the polymer−air−polymer experiment shown in panels a and b in Figure 4. The small quasi-linear Au NP aggregates located inside of the rim (position 2), and the large fractal network on the rim (position 3) are potentially suitable arrangements for SERS[13,18,41−43] of organic moieties such as MV 10B used here. In principle, an organic molecule with a molecular footprint that covers proximal NPs can have their vibrational characteristics enhanced. The higher particle density in these arrangements allows for the presence of the so-called hot spots that are defined by electric field enhancement between closely spaced Au NPs. The hot spots are necessary for SERS given that Raman scattering cross sections for MV 10B are extremely small ($\sim 3.6 \times 10^{-26}$ cm^2 sr^{-1}).[13,44] The coverage, arrangement of the Au NP structures, the planar surface distribution of Au NPs (Figure 4b) and the curvature of the polymer are unaffected by the liquid-based dye during functionalization as shown in Figure S1 in the Supporting Information. The quasi-linear Au NP clusters and the NP networks remain spatially pinned in their original positions.

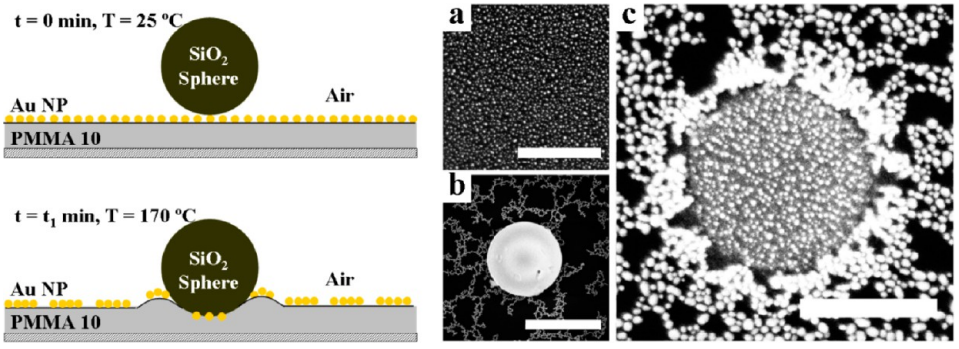

Figure 5. Schematic diagram showing the Au distribution under a spacer before and after heating. (a) SEM image (SB = 200 nm) revealing the Au NP distribution prior to heating. SEM images describing the Au distribution after heating (b) before and (c) after spacer removal. (Scale bars represent 1 μm and 200 nm, respectively.) It can be seen that under the spacer (c) the Au NPs retain their initial uniform distribution as in a. Film polymer thickness is h_{PMMA10} = 26 nm, nominal thickness of the deposit Au layer was h_{Au} = 2 nm, heating time t_1 = 17 min.

dx.doi.org/10.1021/am402285e | ACS Appl. Mater. Interfaces 2013, 5, 8655−8662

Raman scattering measurements of the MV 10B are acquired from the fractal NP network covering the rim (position 3) and the central region inside the structure (position 2) and compared to those from the planar area between the polymer peaks (position 1) in Figure 4c. The spectra reveal that the fractal networks exhibit significant enhancement of the scattering cross-section as the specific Raman-shifts undergo intensity increases and markedly improved resolution (Figure 4c, spectrum 3). The NP arrangement in the central region also exhibits an enhancement (Figure 4c, spectrum 2) but the effect is generally weaker. The primary signatures of the MV, i.e., the main bands enhanced, are at ~1175 (in plane aromatic C−H bending), ~1373 (phenyl C−N stretching and in-plane C−H bending), ~1584 and 1617 cm^{-1} (out−of−phase in plane stretching of the carbon ring atoms).[45] The ratios of the integrated intensities (i.e., the area under each spectrum) are $I_2/I_1 \approx 3$ and $I_3/I_1 \approx 1 \times 10^2$.

The enhancement factor, EF, for each region can be calculated[44,46] using

$$\mathrm{EF} = \frac{I_{\mathrm{SERS}}}{I_{\mathrm{RS}}^{\mathrm{single}}} \frac{1}{N_{\mathrm{CV}} t} \tag{1}$$

For MV dye the contribution of a single dye molecule without surface enhancement to the Raman signal rate is $I_{\mathrm{RS}}^{\mathrm{single}} = 6.3 \times 10^{-7}$ s^{-1}.[46] In the present study a monolayer of dye molecules is assumed to be absorbed onto the substrate (see the Supporting Information). Considering that a MV dye molecule occupies an area of 3.51 nm^2 per molecule[46] implies ~3.12×10^5 molecules are adsorbed in the laser spot area of ~1.1 μm^2. Using the I_{SERS} for the 1617 cm^{-1} peak and considering a uniform monomolecular coverage of the dye the enhancement factors for the regions are found to be $EF_1 \approx 1$, $EF_2 \approx 3$, and $EF_3 \approx 2 \times 10^2$. The enhancement factor calculated for EF_3 is an underestimate as $A_{spot} = 1.1$ μm^2 is larger than the rim area $A_{rim} \approx 0.36$ μm^2 and so contains regions of lower NP density and SERS enhancement (see Figure S1 in the Supporting Information). Accounting for this and considering uniform coverage, EF_3 can be written as the linear contribution of the two regions[46]

$$\mathrm{EF}_3 = \frac{A_{\mathrm{rim}}}{A_{\mathrm{spot}}}\mathrm{EF}_{\mathrm{rim}} + \frac{A_{\mathrm{spot}} - A_{\mathrm{rim}}}{A_{\mathrm{spot}}}\mathrm{EF}_1 \tag{2}$$

Thus, the enhancement factor from the rim alone is estimated to be $EF_{rim} \approx 6 \times 10^2$. As the largest enhancement occurs from the fractal network of NPs on the rim (position 3), this confirms that the rim has the highest density of NPs with proximities that allow electromagnetic field enhancement causing plasmonic coupling and therefore SERS. Conversely those regions with lower enhancement (regions 2 and 1) correspond, in order of decreasing value, to lower NP density.

DISCUSSION

In this study the Au NPs are sputtered onto the surface of the polymer film. Once the polymer films become liquid the particles are free to diffuse and aggregate. The mobility of the NPs on the polymer film influences their aggregation process. Thus, for lower mobility the NP diffusion and aggregation occurs by Ostwald ripening and/or slow coalescence.[23,39] These processes do not seem to be affected by the growth of an electric field induced instability in the polymer film (see Figure 2).

When the NPs are highly mobile, the aggregation process proceeds by initially forming small linear clusters that continue to aggregate and eventually form a fractal network through a diffusion limited process (see ref 24 and the references therein). The presence of an electric field that induces faster changes in polymer surface corrugation seems to enhance this process. This leads to changes in particle density and spatial distribution resulting in fractal clusters (network) on the peaks of the corrugation. The localized fractal formation seems to be associated with an increase in the localized polymer curvature. Thus, in Figures 1 and 3, we note that the fractal is formed either on the peak of the EHD instability (clusters) or on the rims (circular network), whereas in the flat regions between structures, the Au NPs remain organized in quasi-linear clusters. When compared with previous studies presented in ref 24, the values characterizing the particles arrangements (i.e., R_p, d_{ee}, and D) seen on the curved features after $t \approx 21$ or 28 min are similar to those obtained for larger heating times (i.e., $t \geq 135$ min).

The SERS measurements directly confirm the visual changes to the NP density observed in the polymer−air−polymer experiment. The scattering data are consistent with the highest particle density being on the rims, and a greater particle density being inside these structures (position 2) compared to the flat regions (position 1).

In the polymer−air−polymer system, the EHD starts to develop in both films at the same time. As the PS has a smaller viscosity than PMMA, the instability growth is accelerated for PS.[29] Therefore, the instability in PMMA is less developed and its amplitude and curvature is small. The contact with the mirrored features from PS freeze-in the linear Au NPs clusters at an early stage, i.e., well before the fractal is formed (compare Figure 3c with Figure 1d). Once the contact between the mirrored features is formed the PMMA tends to form the shell of the columnar structures (see schematic in Figure 3). The aggregation process continues on the rims where the Au NP movement is not restricted (compare Figure 4b with Figure 3). The presence of SiO_2 sphere also impairs the movement of the NPs from the outset in Figure 5, the NP radius as deposited (R_p = 3.48 nm) being above the critical radius (3.3 nm) that allows for Au clusters to undergo fusion processes on Si substrates.[9] Therefore, NPs maintain their initial randomly uniform distribution (Figure 5a). Essentially, the contact with PS instabilities or SiO_2 microspheres can retard Au NP aggregation on PMMA, and thus control it.

The NP mobility is affected mainly by viscosity of the polymer and the adhesion work between the Au NP and the film, whereas the NP cluster mobility is affected by possible bridges created by the polymer chains between the NPs.[24,47] In the present case, the enhancement in NP and/or cluster mobility in PMMA can be attributed only to a decrease in viscosity as the other two factors that act to reduce the mobility have similar values across the samples. Moreover, the reduced viscosity appears to depend on changes in the local curvature of the polymer film as the aggregation is enhanced in these regions.

Such changes are reported in the literature[27,29,48,49] but are related to changes in the mobility of pristine polymer films. For imprinted features with large aspect ratio and large curvature,[48] such enhancement in polymer mobility is seen only when the feature height is above a certain threshold. A similar threshold is required for the enhancement in the growth rates of the instabilities formed in a polymer−air−polymer system.[29] In the

present case, however, the enhancement of the NP aggregation is seen from the initial stages of the EHD instability where extreme curvatures are not present and the system can be theoretically treated using the long wave approximation.[29] The presence of a surface layer with a lower viscosity is also reported for high-molecular-weight polymers, where entanglement of the polymer chains occurs[27] or when the film thickness is reduced.[29,49] If such an effect is present, it should affect the NP mobility everywhere and would not be limited to the highly curved corrugations of the polymer film as observed here.

The reduction in the film viscosity is also reported to be caused by chain alignment under a thermal field.[50] Such alignments increase with decreasing molecular weight and decreasing film thickness and might be able to induce changes in film mobility in very thin films.[29,51] Here, however, the system is isothermal. Therefore, if present, any alignment that could cause a reduction in viscosity must increase with the curvature. This viscosity decrease could explain the observed enhancement of the NP mobility as the structures are formed.

Finally, it should be mentioned that the method reported here has the significant advantage of patterning the polymer and Au NPs simultaneously. Classical approaches in thin polymer film patterning include the use of top-down photolithography,[52] nanoimprinting[53,54] or e-beam writing,[4] but these techniques are limited by their expensive multistep processes, the development of lithographic, or imprinting masks or by the beam drift and/or its stability.[4] Alternative approaches to creating the required patterns are to incorporate NPs as fillers in thin polymer films, and either use spinodal demixing[1] or induce spinodal[23,24] or EHD[2,3] instabilities to corrugate the air interface of the thin nanocomposite film.

SERS is observed here in the fractal networks of Au NPs formed on the rims of PMMA in a polymer−air−polymer electric field configuration. The enhancement factors of the test molecule spectral components are comparable to those recently reported in the literature for a silicon substrate with evaporated carbon and sputtered gold layers[55] or for clusters in solutions with low dye concentration.[19] Thus, when low dye concentration (1×10^{-6} M) are used in solutions with randomly distributed clusters formed by particles with small radii (7.5−15 nm) enhancement factors of EF $\approx 1\times 10^{1}$ to 1×10^{2} are reported.[19] Here, however, the use of an electric field induced instability allows for patterning of the thin polymer film[25,32] and, therefore, for spatial positioning of the regions with higher Au NP density. Thus, polymer patterns and the high NP density regions can be controlled and anticipated from the outset. This demonstrates that the simple patterning of the polymer by an electric field induced instability associated with densification of NPs around these features can be used as a soft-lithographic technique to create patterned substrates suitable for SERS measurements.

CONCLUSIONS

The present study shows that by inducing an electric field instability in a thin polymer film covered by Au nanoparticles it is possible to form a panoply of patterns at different length scales and spatial positions. It is observed that the rapid growth of a single instability mode from the capillary spectrum due to the applied electric field can have a significant influence on the nanoparticle aggregation process only if the NPs have large mobility on the polymer surface. When they have low mobility, the NPs maintain their initial distribution and the electric field leads to an instability in the polymer film. Higher mobility nanoparticles form fractal clusters or networks spatially organized on the regular pattern in the polymer film induced by the electric field instabilities. The potential for such systems in surface-enhanced Raman spectroscopy is demonstrated by exploiting the beneficial and controllable arrangement of the Au nanoparticles at the same time as the polymer patterning.

ASSOCIATED CONTENT

Supporting Information

The ancillary material contains detailed images showing the nanoparticle clusters and fractal network as seen by the laser spot during the Raman investigation. This material is available free of charge via the Internet at http://pubs.acs.org/.

AUTHOR INFORMATION

Corresponding Author

*E-mail: george.amarandei@ul.ie.

Author Contributions

The manuscript was written through contributions of all authors. All authors have given approval to the final version of the manuscript.

Notes

The authors declare no competing financial interest.

ACKNOWLEDGMENTS

We acknowledge support under EU Framework 7 for projects MRTN-CT-2004005728 (PATTERNS), PERG04-GA-2008-239426 (POLYPATT), and from Tyndall National Institute through Science Foundation Ireland (SFI) funded National Access Programme (Project NAP 200). This work was also supported by SFI under contract 07/SK/B1232a and by the UCC Strategic Research Fund.

ABBREVIATIONS

PS, polystyrene
PMMA, poly(methyl-methacrylate)
NP, nanoparticle
SERS, surface enhanced Raman scattering

REFERENCES

(1) Wong, H. C.; Cabral, J. T. *Phys. Rev. Lett.* **2010**, *105*, 038301.
(2) Bae, J. *J. Ind. Eng. Chem.* **2012**, *18*, 378−383.
(3) Bae, J. W.; Glogowski, E.; Gupta, S.; Chen, W.; Emrick, T.; Russell, T. P. *Macromolecules* **2008**, *41*, 2722−2726.
(4) Goldberg-Oppenheimer, P.; Mahajan, S.; Steiner, U. *Adv. Mater.* **2012**, *24*, OP175−OP180.
(5) Kaune, G.; Ruderer, M. A.; Metwalli, E.; Wang, W.; Couet, S.; Schlage, K.; Röhlsberger, R.; Roth, S. V.; Müller-Buschbaum, P. *ACS. Appl. Mater. Interfaces* **2009**, *1*, 353−360.
(6) Roth, S. V.; Herzog, G.; Körstgens, V.; Buffet, A.; Schwartzkopf, M.; Perlich, J.; Abul Kashem, M. M.; Döhrmann, R.; Gehrke, R.; Rothkirch, A.; Stassig, A.; Wurth, W.; Benecke, G.; Li, C.; Fratzl, P.; Rawolle, M.; Müller-Buschbaum, P. *J. Phys.: Condens. Matter* **2011**, *23*, 254208.
(7) Al-Hussein, M.; Schindler, M.; Ruderer, M. A.; Perlich, J.; Schwartzkopf, M.; Herzog, G.; Heidmann, B.; Buffet, A.; Roth, S. V.; Müller-Buschbaum, P. *Langmuir* **2013**, *29*, 2490−2497.
(8) Faupel, F.; Zaporojtchenko, V.; Strunskus, T.; Elbahri, M. *Adv. Eng. Mater.* **2010**, *12*, 1177−1190.
(9) Schwartzkopf, M.; Buffet, A.; Körstgens, V.; Metwalli, E.; Schlage, K.; Benecke, G.; Perlich, J.; Rawolle, M.; Rothkirch, A.; Heidmann, B.; Herzog, G.; Müller-Buschbaum, P.; Röhlsberger, R.; Gehrke, R.; Stribeck, N.; Roth, S. V. *Nanoscale* **2013**, *5*, 5053−5062.
(10) Cao, Y. C.; Jin, R.; Mirkin, C. A. *Science* **2002**, *297*, 1536−1540.

(11) Cialla, D.; A. März, A.; Böhme, R.; Theil, F.; Weber, K.; Schmitt, M.; Popp, J. *Anal. Bioanal. Chem.* **2012**, *403*, 27−54.
(12) Kneipp, K.; Wang, Y.; Kneipp, H.; Perelman, L. T.; Itzkan, I.; Dasari, R.; Feld, M. S. *Phys. Rev. Lett.* **1997**, *78*, 1667−1670.
(13) Kneipp, K.; Kneipp, H.; Itzkan, I.; Dasari, R.; Feld, M. *J. Phys.: Condens. Matter* **2002**, *14*, R597−R624.
(14) Kleinman, S. L.; Frontiera, R. R.; Henry, A. I.; Dieringer, J. A.; Van Duyne, R. P. *Phys. Chem. Chem. Phys.* **2013**, *15*, 21−36.
(15) Polavarapu, L.; Liz-Marzan, L. M. *Phys. Chem. Chem. Phys.* **2013**, *15*, 5288−5300.
(16) Greeneltch, N. G.; Blaber, M. G.; Henry, A. I.; Schatz, G. C.; Van Duyne, R. P. *Anal. Chem.* **2013**, *85*, 2297−2303.
(17) Ko, H.; Singamaneni, S.; Tsukruk, V. V. *Small* **2008**, *4*, 1576−1599.
(18) Kuo, T. C.; Hsu, T. C.; Y. C. Liu, Y. C.; Yang, K. H. *Analyst.* **2012**, *137*, 3847−3853.
(19) Joseph, V.; Matschulat, A.; Polte, J.; Rolf, S.; Emmerlinga, F.; Kneipp, J. *J. Raman Spectrosc.* **2011**, *42*, 1736−1742.
(20) Adams, S. M.; Campione, S.; Caldwell, J. D.; Bezares, F. J.; Culbertson, J. C.; Capolino, F.; Ragan, R. *Small* **2012**, *8*, 2239−2249.
(21) Seemann, R.; Herminghaus, S.; Jacobs, K. *Phys. Rev. Lett.* **2001**, *86*, 5534−5537.
(22) Thiele, U. In *Thin Films of Soft Matter*; Kalliadasis, S., Thiele, U., Eds.; Springer: Vienna, 2007; p 25.
(23) Amarandei, G.; O'Dwyer, C.; Arshak, A.; Corcoran, D. *Soft Matter* **2013**, *9*, 2695−2702.
(24) Amarandei, G.; O'Dwyer, C.; Arshak, A.; Thiele, U.; Steiner, U.; Corcoran, D. *Langmuir.* **2013**, *29*, 6706−6714.
(25) Schaffer, E.; Thurn-Albrecht, T.; Russell, T. P.; Steiner, U. *Nature* **2000**, *403*, 874−877.
(26) Wu, N.; Russel, W. B. *Nano Today* **2009**, *4*, 180−192.
(27) Barbero, D. R.; Steiner, U. *Phys. Rev. Lett.* **2009**, *102*, 248303.
(28) Goldberg-Oppenheimer, P.; Steiner, U. *Small* **2010**, *6*, 1248−1254.
(29) Amarandei, G.; Beltrame, P.; Clancy, I.; O'Dwyer, C.; Arshak, A.; Steiner, U.; Corcoran, D.; Thiele, U. *Soft Matter.* **2012**, *8*, 6333−6349.
(30) Merkt, D.; Pototsky, A.; Bestehorn, M.; Thiele, U. *Phys. Fluids* **2005**, *17*, 064104.
(31) Voicu, N. E.; Harkema, S.; Steiner, U. *Adv. Funct. Mater.* **2006**, *16*, 926−934.
(32) Morariu, M.; Voicu, N. E.; Schaffer, E.; Lin, Z.; Russell, T. P.; Steiner, U. *Nat. Mater.* **2003**, *2*, 48−52.
(33) Leach, K.; Gupta, S.; Dickey, M.; Willson, C.; Russell, T. P. *Chaos* **2005**, *15*, 047506.
(34) Pototsky, A.; Bestehorn, M.; Merkt, D.; Thiele, U. *Phys. Rev. E.* **2004**, *70*, 025201(R).
(35) Pototsky, A.; Bestehorn, M.; Merkt, D.; Thiele, U. *J. Chem. Phys.* **2005**, *122*, 224711.
(36) Pototsky, A.; Bestehorn, M.; Merkt, D.; Thiele, U. *Europhys. Lett.* **2006**, *74*, 665−671.
(37) Lopes, W. A.; Jaeger, H. M. *Nature* **2001**, *414*, 735−738.
(38) Lopes, W. A. *Phys. Rev. E.* **2002**, *65*, 031606.
(39) Jia, X.; Listak, J.; Witherspoon, V.; Kalu, E. E.; Yang, X.; Bockstaller, M. R. *Langmuir.* **2010**, *26*, 12190−12197.
(40) Fu, T. Z.; Stimming, U.; Durning, C. J. *Macromolecules* **1993**, *26*, 3271−3281.
(41) Fraire, J. C.; Perez, L. A.; Coronado, E. A. *ACS Nano* **2012**, *6*, 3441−3452.
(42) Ganbold, E. O.; Park, J. H.; Dembereldorj, U.; Ock, K. S.; Joo, S. W. *J. Raman Spectrosc.* **2011**, *42*, 1614−1619.
(43) Que, R.; Shao, M.; Zhuo, S.; Wen, C.; Wang, S.; Lee, S. T. *Adv. Funct. Mater.* **2011**, *21*, 3337−3343.
(44) Le Ru, E. C.; Blackie, E.; Meyer, M.; Etchegoin, P. G. *J. Phys. Chem. C.* **2007**, *111*, 13794−13803.
(45) Cyriac, J.; Wleklinski, M.; Li, G.; Gao, L.; Cooks, R. G. *Analyst.* **2012**, *137*, 1363−1369.
(46) Hoflich, K.; Becker, M.; Leuchs, G.; Christiansen, S. *Nanotechnology* **2012**, *23*, 185303.
(47) Cole, D. H.; Shull, K. R.; Baldo, P.; Rehn, L. *Macromolecules* **1999**, *32*, 771−779.
(48) Peng, H. G.; Kong, Y. P.; Yee, A. F. *Macromolecules* **2010**, *43*, 409−417.
(49) Yang, Z.; Fujii, Y.; Lee, F. K.; Lam, C. H.; Tsui, O. K. C. *Science* **2010**, *328*, 1676−1679.
(50) McLeod, E.; Liu, Y.; Troian, S. M. *Phys. Rev. Lett.* **2011**, *106*, 175501.
(51) Cohen, Y.; Reich, S. *J. Polym. Sci. B* **1981**, *19*, 599−608.
(52) Menard, E.; Meitl, M. A; Sun, Y. G.; Park, J. U.; Shir, D. J. L.; Nam, Y. S.; Jeon, S.; Rogers, J. A. *Chem. Rev.* **2007**, *107*, 1117−1160.
(53) Reboud, V.; Kehagias, N.; Zelsmann, M.; Striccoli, M.; Tamborra, M.; Curri, M. L.; Agostiano, A.; Fink, M.; Reuther, F.; Gruetzner, G.; Sotomayor-Torres, C. M. *Appl. Phys. Lett.* **2007**, *90*, 011115.
(54) Tamborra, M.; Striccoli, M.; Curri, M. L.; Alducin, J. A.; Mecerreyes, D.; Pomposo, J. A.; Kehagias, N.; Reboud, V.; Sotomayor-Torres, C. M.; Agostiano, A. *Small* **2007**, *3*, 822−828.
(55) Merlen, A.; Chevallier, V.; Valmalette, J. C.; Patrone, L.; Torchio, P.; Vedraine, S.; Flory, F.; Moula, G. *Surf. Sci.* **2011**, *605*, 1214−1218.